International Journal of Computational Fluid Dynamics

ISSN: 1061-8562 (Print) 1029-0257 (Online) Journal homepage: https://www.tandfonline.com/loi/gcfd20

Hybrid LES-RANS: An approach to make LES applicable at high Reynolds number

Lars Davidson & Simon Dahlström

To cite this article: Lars Davidson & Simon Dahlström (2005) Hybrid LES-RANS: An approach to make LES applicable at high Reynolds number, International Journal of Computational Fluid Dynamics, 19:6, 415-427, DOI: 10.1080/10618560500242280

To link to this article: https://doi.org/10.1080/10618560500242280

International Journal of Computational Fluid Dynamics, Vol. 19, No. 6, August 2005, 415–427

Taylor & Francis
Taylor & Francis Group

Hybrid LES-RANS: An approach to make LES applicable at high Reynolds number

LARS DAVIDSON* and SIMON DAHLSTRÖM

Division of Fluid Dynamics, Department of Applied Mechanics, Chalmers University of Technology SE-412 96, Göteborg, Sweden.
http://www.tfd.chalmers.se/~lada

(Received 10 February 2005; in final form 20 August 2005)

The main bottle neck for using large eddy simulations (LES) at high Reynolds number is the requirement of very fine meshes near walls. Hybrid LES-Reynolds-averaged Navier-Stokes (RANS) was invented to get rid of this limitation. In this method, unsteady RANS (URANS) is used near walls and away from walls LES is used. The matching between URANS and LES takes place in the inner log-region. In the present paper, a method to improve standard LES-RANS is evaluated. The improvement consists of adding instantaneous turbulent fluctuations (forcing conditions) at the matching plane in order to provide the equations in the LES region with relevant turbulent structures. The fluctuations are taken from a DNS of a generic boundary layer. Simulations of fully developed channel flow and plane asymmetric diffuser flow are presented. Hybrid LES-RANS is used both with and without forcing conditions.

Keywords: Large eddy simulations (LES); Reynolds number; Forcing conditions; Turbulent

1. Introduction

When simulating bluff body flows, large eddy simulations (LES) is the ideal method. Bluff body flows are dominated by large turbulent scales which can be resolved by LES without too fine resolution and accurate results can be obtained at affordable cost (Rodi *et al.* 1997, Krajnović and Davidson, 2002, 2003, 2004). On the other hand, doing accurate predictions of wall-bounded flows with LES is a challenging task. The near-wall grid spacing should be about one wall unit in the wall-normal direction. This is similar to the requirement in Reynolds-averaged Navier–Stokes (RANS) using low-Re number models. The requirement for a well-resolved LES in the near-wall region expressed in wall units is approximately 100 (streamwise) and 30 (spanwise). This enables resolution of the near-wall turbulent structures in the viscous sublayer and the buffer layer consisting of high-speed in-rushes and low-speed ejections (Robinson 1991) (often called the streak process). At low to medium Reynolds numbers the streak process generates the major part of the turbulence production. These structures must be resolved in an LES in order to get accurate results. Thus, for wall-bounded flows at high Reynolds numbers of engineering interest, the computational resource requirement of accurate LES is prohibitively large. Indeed, the requirement of near-wall grid resolution is the main reason why LES is too expensive for engineering flows, which was one of the lessons learnt in the LESFOIL project (Davidson *et al.* 2003, Mellen *et al.* 2003).

The object of hybrid LES-RANS (Davidson 2001, Temmerman and Leschziner 2002, Davidson and Peng 2003, Tucker 2003, Xiao *et al.* 2003, Tucker and Davidson 2004) is to get rid of the requirement of high near-wall resolution in wall-parallel planes. In the near-wall region (the URANS region), a low-Re number RANS turbulence model (usually an eddy-viscosity model) is used. In the outer region (the LES region), the usual LES is used. The idea is that the effect of the near-wall turbulent structures should be modelled by the RANS turbulence model rather than being resolved. The matching between the URANS region and the LES region usually takes place in the inner part of the logarithmic region (i.e. around 30–60 wall units away from the wall). In the LES region, coarser grid spacing in wall-parallel planes can be used. In this region the grid resolution is presumably dictated by the requirement of resolving the largest turbulent scales in the flow (which are related to the outer length scales, e.g. the boundary layer thickness), rather than the near-wall turbulent processes. The unsteady momentum equations are solved throughout the computational domain. The turbulent RANS viscosity is used in the URANS region, and the turbulent SGS viscosity is used in the LES region.

*Corresponding author. Email: lada@chalmers.se

International Journal of Computational Fluid Dynamics
ISSN 1061-8562 print/ISSN 1029-0257 online © 2005 Taylor & Francis
http://www.tandf.co.uk/journals
DOI: 10.1080/10618560500242280

Recent work on hybrid LES-RANS can be found in (Davidson 2001, Temmerman and Leschziner 2002, Davidson and Peng 2003, Hamba 2003, Tucker 2003, Xiao *et al.* 2003, Tucker and Davidson 2004). In Davidson (2001), Davidson and Peng (2003), Hamba (2003), Xiao *et al.* (2003) two-equation models were used in the URANS region and a one-equation SGS model was employed in the LES region. One-equation models were used in both regions in Tucker (2003), Tucker and Davidson (2004). The locations of the matching planes were determined in different ways. In some works (Davidson 2001, Davidson and Peng 2003, Hamba 2003), it was chosen along a pre-selected grid plane. In Tucker and Davidson (2004) it was determined by comparing the URANS and the LES turbulent length scales or it was computed from turbulence/physics requirements. Xiao *et al.* (2003) used a two-equation model in the URANS region and blended it into a one-equation in the LES region. In Tucker (2003) different partial differential equations for automatically finding the matching plane were investigated.

Hybrid LES-RANS is similar to detached eddy simulations (DES) (Spalart *et al.* 1997, Spalart 2000, Strelets 2001). The main difference is that the original DES aims at covering the whole attached boundary layer with URANS, whereas hybrid LES-RANS aims at covering only the inner part of the boundary layer with URANS. In later work DES has been used as a wall model (Nikiton *et al.* 2000, Piomelli *et al.* 2003), and in this form DES is very similar to hybrid LES-RANS.

Although good results have been presented with hybrid LES-RANS, it has been found that the treatment of the interface between the RANS region and the LES region is crucial for the success of the method. The resolved turbulence supplied by the URANS region to the LES region does not have any reasonable turbulent characteristics and is not representative of turbulence at all. This results in too poorly resolved stresses on the LES side of the interface and this gives a hack—also referred to as a shift—in the velocity profile approximately at the location of the matching plane (Nikiton *et al.* 2000, Davidson 2001, Temmerman and Leschziner 2002, Davidson and Peng 2003, Hamba 2003, Piomelli *et al.* 2003, Dahlström 2003, Tucker and Davidson 2004). The too low-resolved stresses in the LES region gives too a small wall shear stress. Several modifications have been proposed to remove this deficiency. Temmerman and Leschziner (2002) proposed to dampen the modelled stresses in the URANS region to reduce the total (i.e. resolved plus modelled) shear stress in the URANS region and thereby, reducing the jump in shear stress across the matching plane. In Tucker and Davidson (2004) numerical smoothing was used at the interface. Hamba (2003) proposed a modification of the discretized streamwise equation at the interface in order to avoid filtering out any resolved fluctuations. In Piomelli *et al.* (2003) backscatter was introduced in the interface region with the object to generate resolved turbulent fluctuations.

In the present paper, we propose to add fluctuations to the momentum equations at the LES side of the interface (Dahlström 2003, Dahlström and Davidson 2003). The turbulent fluctuations $u'_{\mathrm{DNS}}, v'_{\mathrm{DNS}}, w'_{\mathrm{DNS}}$ are taken from a DNS of a generic boundary layer. The aim is to create resolved turbulence with reasonable structural information of relevant time and length scales. The added fluctuations act as a forcing term $-u'_{2,\mathrm{DNS}}u'_{i,\mathrm{DNS}}/\Delta y$ in the $\bar{u}_i$ momentum equations. The time-averaged source in the streamwise momentum equation is positive (i.e. $-\langle u'_{\mathrm{DNS}}v'_{\mathrm{DNS}}\rangle > 0$), and the added momentum diffuses towards the wall and increases the wall shear stress. An interesting—and rather similar approach—was recently presented by Batten *et al.* (2004) in which synthetic turbulent fluctuations were used to trigger the resolved turbulence when going from an URANS region to an LES region.

In the present paper, the improved LES-RANS method is discussed and results from channel flow predictions at different Reynolds numbers as well as predictions of the flow in an asymmetric, plane diffuser are presented.

2. Equations

The Navier-Stokes equations with an added turbulent/SGS viscosity read

$$\frac{\partial \bar{u}_i}{\partial t} + \frac{\partial}{\partial x_j}(\bar{u}_i\bar{u}_j) = \beta\delta_{1i} - \frac{1}{\rho}\frac{\partial \bar{p}}{\partial x_i} + \frac{\partial}{\partial x_j}\left[(\nu + \nu_T)\frac{\partial \bar{u}_i}{\partial x_j}\right] \quad (1)$$

$$\frac{\partial \bar{u}_i}{\partial x_i} = 0 \quad (2)$$

where $\nu_T = \nu_t$ (ν_t denotes the turbulent RANS viscosity) for $y \le y_{ml}$ (see figure 1), otherwise $\nu_T = \nu_{sgs}$. The coefficient $\beta = 1$ for channel flow simulations with periodic streamwise boundary conditions; otherwise it is zero. The density is set to one in all simulations.

2.1 URANS vs. LES

The bar ($\bar{\cdot}$) over the velocity components and pressure in equations 1 and 2 denotes time (or ensemble) averaging in the URANS region and implicit filtering (i.e discretization) in the LES region. Thus the flow variables in the URANS region and in the LES region are defined in different ways. Does this pose any problems? Formally it may seem worrying that the flow variables are filtered in one region and time averaged in another. On the other hand, how does equation 1 know if it has been filtered or time averaged? The answer is it does not. The form of the equation and its boundary conditions are identical on filtered and time-averaged form. Actually, the only way equation 1 feels if its describing an LES flow or an URANS flow is through ν_T, which we expect to be larger in URANS than in LES. But we cannot know for sure: if a large Δ in the SGS model is chosen (i.e. larger than the control volume), ν_T may well be large also for LES (Davidson and Peng 2003).

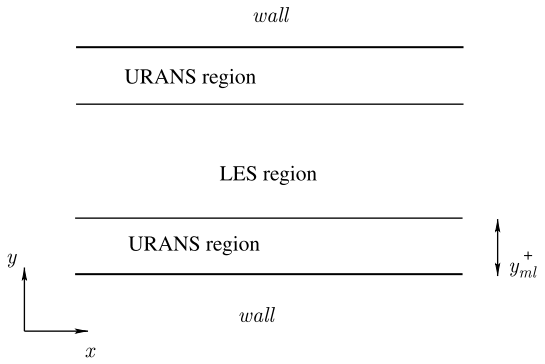

Figure 1. The LES and URANS region.

However, usually there is a difference in how the turbulent viscosity is computed in URANS and LES. The turbulent viscosity can be expressed as $\nu_T \propto \mathcal{U}\ell$, where $\mathcal{U}$ and ℓ denote a characteristic turbulent velocity and length scale, respectively. In LES, the length scale is related to the filter width, which is commonly taken as proportional to a characteristic length of the computational cell. In URANS, however, the turbulent length scale is obtained by solving a transport equation (for example an equation for ε or ω). Sometimes, as in the URANS region in the present work, the length scale is taken as being proportional to the distance from the nearest wall. The velocity scale in LES is either taken from the strain rate and the filter width, i.e. $(\bar{s}_{ij}\bar{s}_{ij})^{1/2}\Delta$ or by solving a transport equation for the SGS turbulent kinetic energy k_{sgs}. In URANS, the turbulent velocity scale is obtained by solving a transport equation for the turbulent kinetic energy k.

2.2 Boundary conditions

No-slip conditions are used at the walls and periodic boundary conditions are used in the spanwise direction (z). Neumann boundary conditions are used for pressure at all boundaries. Periodic boundary conditions in the streamwise direction (x) are employed in most of the channel simulations. In one channel simulation and in the diffuser simulations the inlet condition is taken from a separate channel DNS at $Re_\tau = 500$.

The turbulent kinetic energy k_T (equation 6) is set to zero at all walls. Since the inlet value of k_T-equation is unknown, Neumann conditions are used at the inlet, i.e. $\partial k_T/\partial x = 0$. Some tests with $k = 0$ at the inlet have been carried out and no noticeable influence on the predictions was found.

3. The numerical method

Second-order central differencing in space is used for all terms. An implicit, two-step time-advancement method is employed for the pressure–velocity coupling. The discrete form of equation 1 can be written as

$$\bar{u}_i^{n+1/2} = \bar{u}_i^n + \Delta t H\left(\bar{u}_i^n, \bar{u}_i^{n+1/2}\right) - \frac{1}{\rho}\alpha\Delta t\frac{\partial \bar{p}^{n+1/2}}{\partial x_i} - \frac{1}{\rho}(1-\alpha)\Delta t\frac{\partial \bar{p}^{n}}{\partial x_i} \tag{3}$$

where $H(\bar{u}_i^n, \bar{u}_i^{n+1/2})$ includes the convection term, the driving pressure gradient, the viscous and the turbulent stresses, and $\alpha = 0.5$ (the Crank-Nicolson scheme). Equation 3 gives $\bar{u}_i^{n+1/2}$ which does not satisfy continuity. An intermediate velocity field is computed by subtracting the implicit part of the pressure gradient, i.e.

$$\bar{u}_i^* = \bar{u}_i^{n+1/2} + \frac{1}{\rho}\alpha\Delta t\frac{\partial \bar{p}^{n+1/2}}{\partial x_i}. \tag{4}$$

Now $\bar{u}_i^{n+1/2}$ and $\bar{p}_i^{n+1/2}$ in equation 4 are replaced by the velocity and pressure fields at level $(n+1)$, i.e. $\bar{u}_i^{n+1}$ and $\bar{p}_i^{n+1}$. Taking the divergence of equation 4 and requiring that the face velocities $\bar{u}_{i,f}^{n+1}$ (which are obtained by linear interpolation) satisfy the continuity equation the following Poisson equation for pressure is obtained

$$\frac{\partial^2 \bar{p}^{n+1}}{\partial x_i \partial x_i} = \frac{\rho}{\Delta t\alpha}\frac{\partial \bar{u}_{i,f}^*}{\partial x_i}. \tag{5}$$

The Poisson equation is solved with an efficient multigrid method (Emvin 1997). For more details, see Davidson and Peng (2003).

It should be mentioned that some convergence/oscillation problems were encountered for the diffuser flow. This problem was fixed by using slightly implicit time discretization for the pressure, i.e. $\alpha = 0.7$. The Crank-Nicolson scheme was used for all other terms. These convergence/oscillation problems are believed to be related to the inlet boundary conditions (instantaneous DNS data) used for the diffuser flow.

4. The Hybrid LES-RANS model

A one-equation model is employed in both the URANS region and LES region which reads

$$\frac{\partial k_T}{\partial t} + \frac{\partial}{\partial x_j}(\bar{u}_j k_T) = \frac{\partial}{\partial x_j}\left[(\nu + \nu_T)\frac{\partial k_T}{\partial x_j}\right] + P_{k_T} - C_\varepsilon\frac{k_T^{3/2}}{\ell} \tag{6}$$

$$P_{k_T} = 2\nu_T\bar{s}_{ij}\bar{s}_{ij}$$

In the inner region ($y \le y_{ml}$) k_T corresponds to RANS turbulent kinetic energy k; in the outer region ($y > y_{ml}$) it corresponds to subgrid-scale kinetic turbulent energy (k_{sgs}). No special treatment is used in the equations at the matching plane except that the form of the turbulent

Table 1. Turbulent viscosities and turbulent length scales in the URANS and LES regions.

	URANS region	LES region
ℓ	$2.5n[1-\exp(-0.2k^{1/2}n/\nu)]$	$\ell=\Delta=(\delta V)^{1/3}$
ν_T	$2.5k^{1/2}n[1-\exp(-0.014k^{1/2}n/\nu)]$	$0.07k_{sgs}^{1/2}\ell$
C_ε	1.0	1.07

n denotes the distance to the nearest wall.

viscosity and the turbulent length scale are different in the two regions, see table 1.

4.1 Forcing conditions

Although much better results are obtained on coarse meshes compared to LES, conventional zonal hybrid LES-RANS needs to be improved. First, the method is sensitive to the location of the interface. Second, ideally, modelled turbulence in the URANS region should through the matching plane be transformed to resolved turbulence. This does not occur and this means that the LES region is supplied with poor boundary conditions from the URANS region. Although the flow coming from the URANS region indeed is unsteady (it is triggered by the LES region), the resolved flow coming from the URANS region does not have any proper turbulent structures. The length scales and time scales of the unsteadiness in the URANS region are not related to large-scale turbulence, because a large part of the turbulence in the URANS region is modelled. Since near-wall turbulence is characterized by violent low-speed outward ejections and high-speed in-rushes (Robinson 1991), it can be expected that it is important that the characteristics of the turbulent structures are transferred to the LES region. If real turbulence, for example from a DNS, were supplied to the LES region along the interface plane as instantaneous velocity and pressure, the quality of the LES predictions in the LES region would—as in usual LES—depend on the SGS model and the grid resolution. In Baggett (1997) channel flow DNS was studied, where the computational domain near one wall was omitted, and along this boundary exact boundary conditions from a previous DNS were supplied. As expected results identical to the DNS of the complete channel were obtained. It was found that the boundary conditions could be slightly modified without affecting the predicted results, as long as the structural information in the boundary conditions was not lost.

In the present work, an improved hybrid LES-RANS (Dahlström 2003, Dahlström and Davidson 2003) is employed in which forcing is applied at the interface. Sources including turbulent velocity fluctuations are added to the three momentum equations in the LES region in the cells adjacent to the interface. The fluctuations $u'_{DNS}, v'_{DNS}, w'_{DNS}$ are obtained from a channel DNS ($Re_\tau=500$), in which the velocity field along the line $x=x_0$, $y=y_{ml}$ every time step was stored on disk. Fluctuations $u'_{i,DNS}(x_0,y_{ml},z,t)$ are used to compute the source

$$S_i=-\gamma\rho u'_{i,DNS}u'_{j,DNS}\delta_{j2}A_n=-\gamma\rho\frac{u'_{i,DNS}u'_{2,DNS}}{\Delta y}\Delta V \quad (7)$$

in the $\bar{u}_i$ momentum equation. A_n and ΔV denote the area and the volume of the control volume respectively, see figure 2, and γ is a scaling function which is the ratio of the local modelled turbulent kinetic energy and the turbulent kinetic energy of the added DNS fluctuations, i.e.

$$\gamma(x,y_{ml},z,t)=\frac{c_\gamma k(x,y_{ml},z,t)}{\left[0.5(u^2_{DNS,rms}+v^2_{DNS,rms}+w^2_{DNS,rms})\right]} \quad (8)$$

with $c_\gamma=0.4$. This expression is slightly different from that used in Dahlström (2003), Dahlström and Davidson (2003). The channel predictions with periodic streamwise boundary conditions are fairly sensitive to how equation 8 is chosen. However, the channel simulations with inlet/outlet boundary conditions as well as the diffuser flow are much less sensitive to the exact form of equation 8.

Taylor's hypothesis is used to achieve streamwise variation of the DNS fluctuations in equation 7, i.e.

$$u'_{DNS}(x,y_{ml},z,t)=u'_{DNS}(x_0,y_{ml},z,\tau),$$
$$\tau=M_{DNS}(t-(x-x_0)/V_S),\quad V_S=\langle\bar{u}_{y_{ml}}\rangle \quad (9)$$

A low M_{DNS} value gives an increased streamwise turbulent length scale. In Davidson and Billson (2004) different values of M_{DNS} were evaluated, and it was found that $M_{DNS}=0.25$ gave the best result. This M_{DNS}-value gives a streamwise integral length scale $\mathcal{L}_x$ of the added DNS fluctuations which is approximately four times too large. However, the magnitude of the true $\mathcal{L}_x$ is similar to the streamwise grid spacing. It makes no sense adding fluctuations whose integral length scale is close to the streamwise length scale (i.e. with $\mathcal{L}_x\simeq\Delta x$), as the equations cannot respond to a forcing with such a small length scale. This is probably the reason why the results are improved when the streamwise integral length scale of the added fluctuations is increased by a factor of four.

One important difference between the numerical experiment in Baggett (1997) and the present hybrid LES-RANS is that in the former case the flow equations are not solved for in the near-wall region, but in the present method, the URANS equations are solved. Thus, in the present method the equations in both the LES and URANS regions are allowed to respond to the added fluctuations in their non-linear fashion. This is believed to be very important.

4.2 Direct numerical simulations

To generate DNS-fluctuations for the inlet boundary conditions and the forcing described, a DNS of channel flow at $Re_\tau=500$ was carried out. The finite volume method presented above was used. A $64\times64\times64$ mesh was employed. The extent of the computational domain was

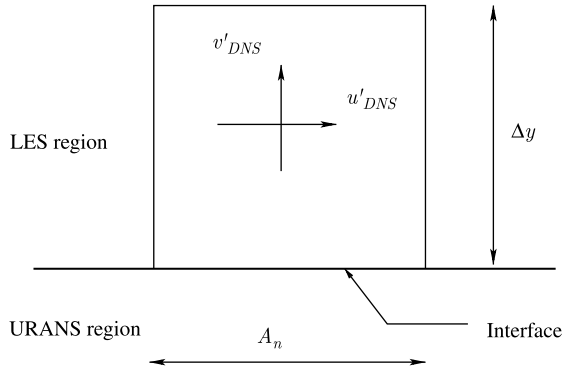

Figure 2. Added fluctuations (u'_{DNS}, v'_{DNS} and w'_{DNS}) in a control volume ($j_{ml}+1$) in the LES region adjacent to the interface.

$2\pi \times 2 \times 0.5\pi$ (x, y, z). The first near-wall computational node was located at $y^+ = 0.3$ and the geometric stretching in the y direction was 17%.

The streamwise velocity profile and the resolved RMS fluctuations are in figure 3 compared with the DNS in Moser *et al.* (1999) at $Re_\tau = 395$ and $Re_\tau = 595$. As can be seen, the agreement is reasonable.

Instantaneous data of U, V and W at plane x_0 are stored at disk. They are stored during 5000 time steps (occupying approximately 1 GB of disk). These data are used for prescribing instantaneous inlet data for the channel flow with inlet/outlet boundary conditions as well as for the diffuser flow. Instantaneous data along a z line at the appropriate y^+ locations are used for the forcing conditions. When time corresponding to step 5000 is reached, we cycle through the data backward and so on.

It is believed that these data can be used for forcing at the interface for a wide range of boundary layers. The turbulence structure in the inner logarithmic region is only weakly dependent on Reynolds number. It can be noted that the data used for forcing at the interface possess realistic structural information. One aspect of this is shown in figure 4 in which a scatter plot for quadrant analysis of the u' and v' fluctuations at $y^+ = 60$ is presented. As expected, quadrant 2 (negative u' and positive v') and quadrant 4 (positive u' and negative v') are dominating. The events corresponding to these two quadrants contribute to negative $\langle u'v' \rangle$ correlation. It can also be seen that the contribution to $-\langle u'v' \rangle$ is larger for quadrant 2 than for quadrant 4, which is in agreement with other DNS (Kim *et al.* 1987) and experiments (Alfredsson and Johansson 1984).

5. Results

Results from two configurations are presented, namely channel flow and the flow in an asymmetric diffuser.

5.1 Channel flow simulations

The grids used in the present study are coarse, see table 2, in order to investigate how well hybrid LES-RANS works on such grids. The Reynolds number is defined as $Re_\tau = u_\tau \delta/\nu$, where δ denotes channel half width and u_τ denotes friction velocity related to the driving pressure gradient. $\langle \cdot \rangle$ denotes time, spanwise and streamwise averaging when periodic streamwise conditions are used. When inlet/outlet boundary conditions are used in the streamwise direction, $\langle \cdot \rangle$ denotes time and spanwise averaging. In figures 5 and 6 the predicted velocity profiles from channel flow simulations obtained with hybrid LES-RANS with and without forcing are presented. Different locations of the matching plane are used ($y^+_{ml} = 34$, 62 and 126) and different Reynolds numbers ($Re_\tau = 500$, 2000 and 4000). Both the LES-simulations and the hybrid LES-RANS for $Re_\tau = 500$ yield a laminar solution due to the low Reynolds number and the poor resolution (figure 6). As can be seen, the hybrid LES-RANS with forcing conditions give much better velocity profiles than without forcing conditions. For $y^+_{ml} = 62$ and 126 (figure 5a) and for $Re_\tau = 2000$ and 4000 (figure 6a) the agreement is excellent.

Note that the net force in the streamwise direction is positive, i.e. $S_1 = -\gamma \rho A_n \langle u'_{1,DNS} u'_{2,DNS} \rangle > 0$, see equation 8. In the inner log-law region, the numerical value of $-\langle u'_{1,DNS} u'_{2,DNS} \rangle / u_\tau^2$ ranges between 0.3 and 0.5. This force can be seen as a compensation for the fact that

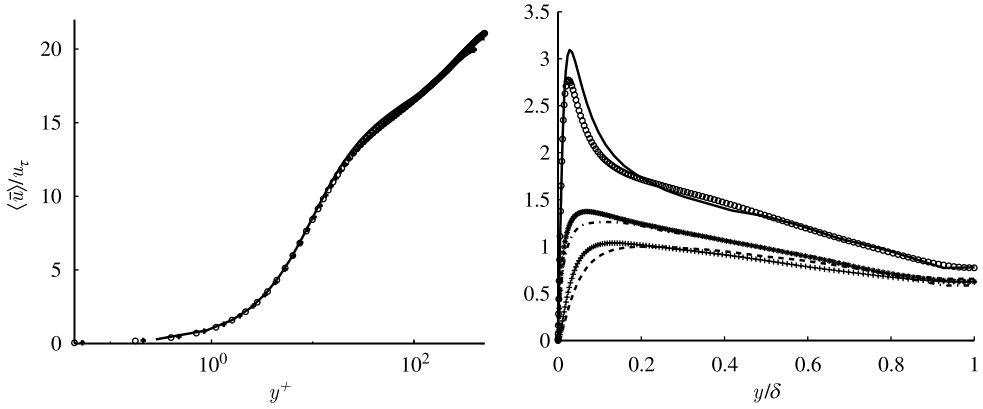

(a) Velocity profile. Lines: present DNS; ○: Re_τ = 595; +: Re_τ = 395

(b) RMS fluctuations. Lines: present DNS; markers: Re_τ = 595

Figure 3. Streamwise $\langle \bar{u} \rangle$ profiles and resolved RMS fluctuations. Lines: present DNS; markers: DNS [24].

Table 2. Channel flow. $x_{max} = 4\pi$, $z_{max} = \pi$.

Re_τ	B.C.	y_{ml}/δ	y^+_{ml}	j_{ml}	$u_{*,w}$	Δx^+	Δz^+	ny	f_y
500	inlet/outlet	0.075	38	17	0.9	196	98	64	1.17
500	Periodic	0.122	60	16	1.10	196	98	64	1.12
2000	Periodic	0.017	34	9	1.13	785	393	64	1.17
2000	Periodic	0.031	62	12	1.14	785	393	64	1.17
2000	Periodic	0.063	126	16	1.15	785	393	64	1.17
4000	Periodic	0.016	64	13	1.15	1571	785	80	1.15

The meshes have 32 cells in streamwise (x) direction and 16 cells in spanwise (z) direction. ny and f_y denote number of cells and geometric grid stretching in y direction, respectively. y_{ml} denotes position of the matching plane between the LES and URANS regions. The $j_{ml} - 1$ value represents number of cells in one URANS region. The boundary condition (B.C.) in the streamwise direction is either inlet/outlet or periodic. For the inlet/outlet case $Re_\tau = 500$ at the inlet.

the streak process consisting of high-speed in-rushes and low-speed ejections are poorly captured by the turbulence model in the URANS region. When streamwise periodic conditions are used (prescribed Re_τ), this means that the wall shear stress at the walls will not be balanced by the driving pressure gradient, but now the global momentum balance together with the forcing condition reads (equation 1 with $\beta = 1$ integrated from (0,0,0) to ($x_{\max}$, 2δ, $z_{\max}$))

$$2\delta x_{\max} z_{\max} - \gamma \langle u'_{1,DNS} u'_{2,DNS} \rangle 2\delta x_{\max} z_{\max} = \tau_w 2\delta x_{\max} z_{\max} \quad (10)$$

Since $-\langle u'_{1,DNS} u'_{2,DNS} \rangle > 0$, we get $\tau_w = \rho u^2_{*,w} > 1$. The friction velocity $u_{*,w}$ is given in table 2. When inlet/outlet boundary conditions are used, the situation is slightly different since in this case it is the mass flow which is prescribed (Re_b) and the friction velocity (Re_τ) is part of the solution. Figures 7 and 8 present the three terms in the averaged streamwise momentum equation, the total (viscous plus turbulent) diffusion term, the pressure gradient and the Reynolds stress. Note that all terms are scaled with $\tau_w = \rho u^2_{*,w}$. As can be seen, with forcing conditions (figures 7a and 8a), the added momentum force S_1 is taken up by the diffusion term and the added momentum is transported to the wall to satisfy equation 10. This takes place for both types of streamwise boundary conditions (periodic or inlet/outlet). The jump in the diffusion profile corresponds to the added momentum source S_1. The jump—and thus S_1—is slightly larger for the periodic case $\left(y^+_{ml} = 62\right)$ mainly because the matching planes are located at different locations and $-\langle u'_{DNS} v'_{DNS} \rangle$ is larger at $y^+ = 62$ than at $y^+ = 38$.

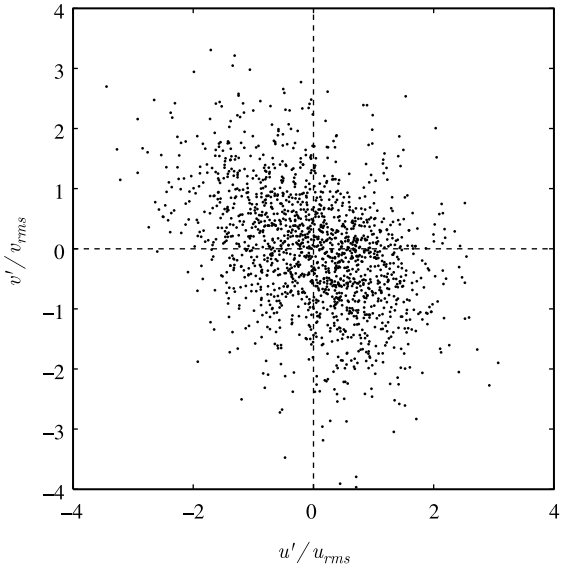

Figure 4. Scatter plot of u' and v' fluctuations at $y^+ = 60$. Present DNS.

The added fluctuations also act as an additional production term $-0.5\langle \gamma u'_{i,DNS} u'_{2,DNS} u'_i \rangle / \Delta y$ in the equation for the resolved turbulent kinetic energy, the $0.5\langle u'_i u'_i \rangle$ equation. The additional production term is large compared to the local resolved production, see figure 9a, even though the correlation between the added DNS fluctuations and the resolved fluctuations is very weak, see figure 9b. For example, the correlation coefficient between the streamwise DNS fluctuation and the resolved wall-normal fluctuation is $\langle u'_{DNS} v' \rangle / (u_{DNS,rms} v_{rms}) = 0.078$. The kink in the profile of the resolved production in figure 9a stems from the kink in the shear stress profiles $\langle u'v' \rangle$, see figures 7a and 8a.

The added DNS fluctuations thus act as a source both in the momentum equations and the resolved turbulent kinetic energy. This is contrary to the method in Piomelli *et al.* (2003), where white noise was added in the interface region. Their source to the turbulent kinetic energy was substantial but the source to the momentum equation was negligible.

In figure 10a the resolved and modelled turbulent kinetic energies are shown. One interesting feature should be noticed first: the resolved, turbulent kinetic energy is, when going from the URANS region to the LES region across the matching plane (located at $y/\delta = 0.031$, see table 2), reduced when forcing conditions are used. This does not happen when no forcing conditions are used. The ratio of resolved and modelled shear stress, on the other hand, is in the LES region larger with forcing conditions than without, see figures 7 and 8. This indicates that some structural information is imposed on the turbulence by the forcing conditions, and that the added DNS fluctuations increase the correlation between the resolved fluctuations. The larger shear stress gradient with forcing conditions increase the momentum transport toward the center, which prevents the over-prediction of the velocity in the center which is seen for the non-forcing case, see figures 5 and 6.

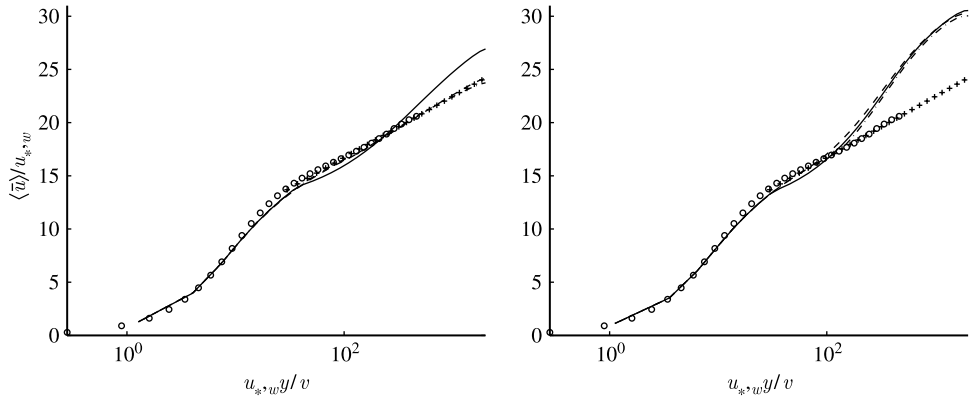

(a) With forcing conditions. (b) Without forcing conditions.

Figure 5. $\langle\bar{u}\rangle$ profiles. $Re_\tau = 2000$. Streamwise periodic boundary conditions. Interface plane at different locations. Solid lines: $y^+_{ml} = 34$; dashed lines: $y^+_{ml} = 62$; dash-dotted lines: $y^+_{ml} = 126$; ○: present DNS; + : $2.5 \ln(y^+) + 5.2$.

The turbulent viscosities in the LES region are large (figure 10b), much larger than in a wall-resolved LES. It can be noted that the turbulent viscosity in the URANS region is not much larger than in the LES region. It is also seen that the ratio $\langle\nu_T\rangle/\nu$ increases for increasing Reynolds number which is to be expected.

In figure 11 the RMS fluctuations are presented. Again, it is seen that the RMS fluctuations with forcing conditions decrease in the LES region compared to the URANS region (at least the streamwise and the spanwise). The peaks of the u_{rms} and w_{rms} profiles are located close to the matching plane. The corresponding peaks for the non-forcing case are located far out in the LES region. The v_{rms} profiles for the forcing and non-forcing case are fairly similar, except that the peak is somewhat larger for the forcing case. Hence, it seems that the added DNS fluctuations influence the $\bar{u}$ and $\bar{w}$ equations such that realistic resolved u_{rms} and w_{rms} are obtained, but not so for v_{rms}. The reason for this is not clear. When comparing turbulent quantities for the forcing and the non-forcing case, it should be recalled that all turbulent quantities have been scales with $u_{*,w}$ which is one for the non-forcing case, but is larger than one for the forcing case (see table 2).

A drawback with hybrid LES-RANS which has not been mentioned is that the total RMS fluctuations, i.e. the modelled plus the resolved, are much too large, see figures 10a and 11. Usually this is no big issue, since in most applications it is sufficiency if the mean flow quantities are well predicted.

5.2 *Diffuser flow simulations*

The configuration is an asymmetric plane diffuser, see figure 12, with Reynolds number $Re = U_{b,in}H/\nu = 18{,}000$ ($U_{b,in} = H = 1$). The opening angle is 10°. Instantaneous

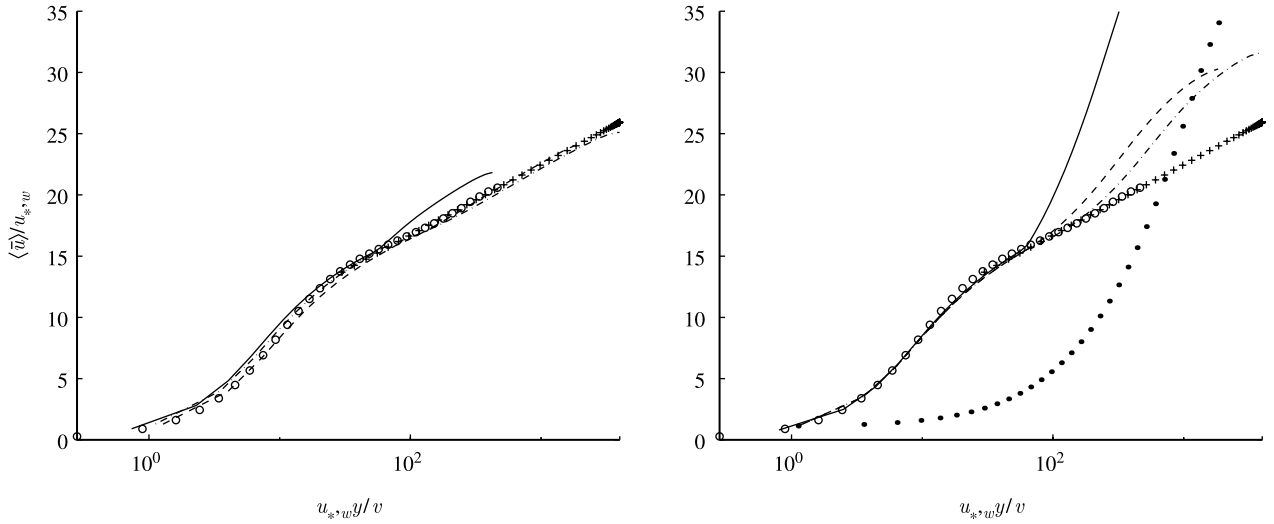

(a) With forcing conditions. (b) Without forcing conditions.

Figure 6. $\langle\bar{u}\rangle$ profiles. Streamwise periodic boundary conditions. $y^+_{ml} \simeq 60$. Solid line: $Re_\tau = 500$; dashed line: $Re_\tau = 2000$; dash-dotted line: $Re_\tau = 4000$; dotted line [in figure b)]: LES at $Re_\tau = 2000$; ○: present DNS; + : $2.5 \ln(y^+) + 5.2$.

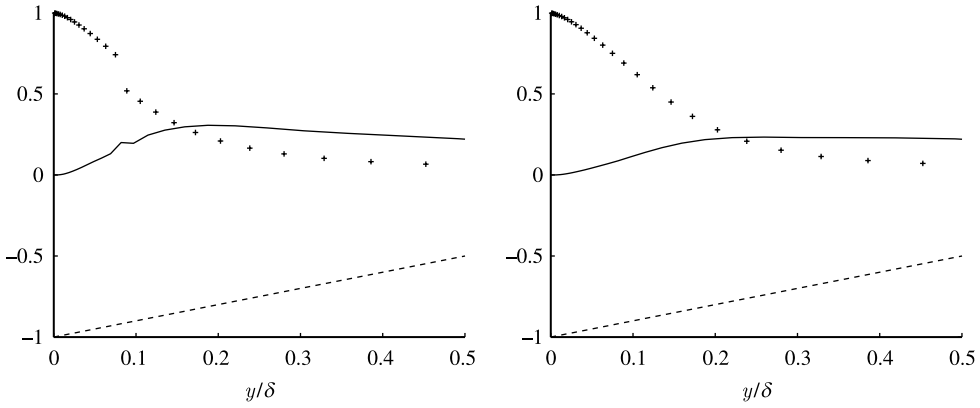

(a) With forcing conditions. (b) Without forcing conditions.

Figure 7. Terms in the $\langle \bar{u} \rangle$ equation. $Re_\tau = 500$, $y^+_{ml} = 38$. Inlet/outlet boundary conditions in streamwise direction. Solid line: $\langle -u'v' \rangle / u^2_{*,w}$; +: $\langle (\nu + \nu_T) \partial \bar{u} / \partial y \rangle / u^2_{*,w}$; dashed lines: streamwise pressure gradient and $\tau_w / u^2_{*,w}$.

inlet boundary conditions are prescribed using the present channel DNS (figure 3) and convective boundary conditions are used at the outlet. Periodic boundary conditions are prescribed in the spanwise direction. The mesh has $256 \times 64 \times 32$ (x, y, z) cells (body-fitted, structured, nearly orthogonal mesh), which gives a spanwise resolution at the inlet of $\Delta z^+ \simeq 120$. The CPU time is approximately 12 s per time step on a Linux PC (AMD 2200+). A time step of 0.04 is used ($CFL_{max} \simeq 1$) and to reach convergence two global iterations are needed at each time step. The discretized equations are consider to have converged when the residual $\epsilon_\Phi (\epsilon_\Phi = \sum_{\text{all cells}} |\text{RHS} - \text{LHS}|)$, scaled with the total inflow of variable Φ is smaller than 0.001 ($\Phi = 1$[continuity], $\bar{u}$, $\bar{v}$, or $\bar{w}$). A typical run restarts from a previous calculation; 15,000 times steps are used to get fully developed flow and statistics is then gathered for another 15,000 times steps.

Figure 13 presents the velocity profiles. The agreement is good, both with and without forcing conditions. Both models slightly underpredict the peak in the region $14H < x < 20H$. Furthermore, it can be seen that at $x = 6H$ the flow predicted without forcing conditions the peak velocity is slightly overpredicted and consequently the separation is predicted too early. Consequently the re-attachment takes place earlier without than with forcing conditions, and the recovery of the boundary is fortuitously better predicted without than with forcing conditions. Still, considering the poor predictions obtained without forcing conditions for the channel flow simulations, the predictions of the diffuser flow without forcing conditions are surprisingly good. The reason is probably that the flow is supplied with proper turbulent structures at the inlet (the channel DNS fluctuations), and these turbulent structures are still present in the flow when it enters the diffuser region.

In figure 14 the velocity profiles computed with pure LES with a one-equation SGS model are presented. The velocity profiles in the entrance of the diffuser are very poor. However, further downstream the LES-results agree well with experiments, but this must be regarded as purely coincidental, considering the very poor predictions further upstream.

The location of the matching plane is chosen at the inlet at $y^+_{ml} = 34$ (both for lower and upper wall). This corresponds to ten cells in the upper and lower URANS regions. Downstream, the location of the matching plane

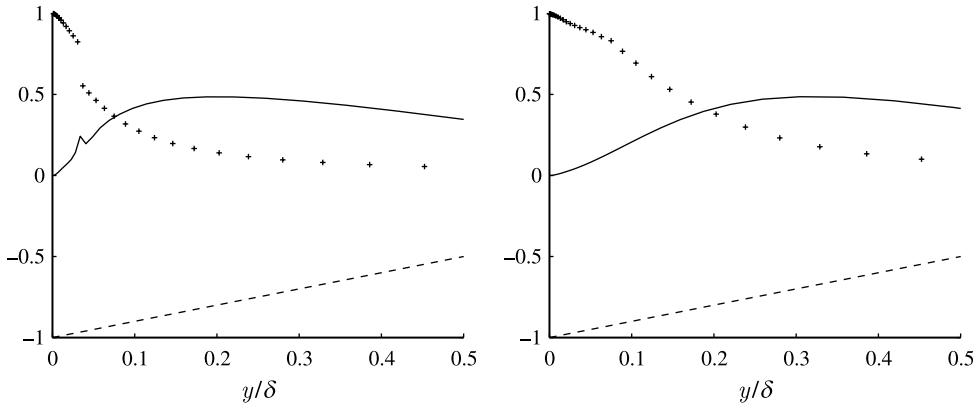

(a) With forcing conditions. (b) Without forcing conditions.

Figure 8. Terms in the $\langle \bar{u} \rangle$ equation. $Re_\tau = 2000$, $y^+_{ml} = 62$. Streamwise periodic boundary conditions. Solid line: $\langle -u'v' \rangle / u^2_{*,w}$; +: $\langle (\nu + \nu_T) \partial \bar{u} / \partial y \rangle / u^2_{*,w}$; dashed lines: streamwise pressure gradient and $\tau_w / u^2_{*,w}$.

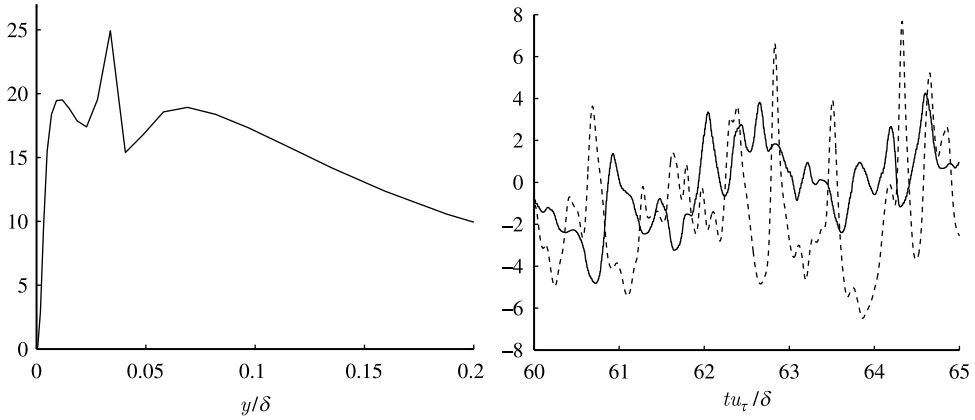

(a) Resolved production $-\langle u'v'\rangle\,\partial\langle u\rangle/\partial$y. The production due to the imposed DNS fluctuations $-0.5\gamma\langle u'_{i,DNS}u'_{2,DNS}u'_i\rangle/\Delta y \simeq 170$.

(b) Time history of streamwise velocity fluctuation in a control volume in the LES region adjacent to the interface (cell $j_{ml}+1$). Solid line: u'_{DNS}; dashed line: u'.

Figure 9. Channel flow. $Re_\tau = 2000$. Streamwise periodic boundary conditions with forcing conditions. $y^+_{ml} = 62$.

is computed by requiring that the volume flow rate in the URANS region should be the same at all x. For the lower wall $j_{ml,i}$ is computed from

$$U_{b,\mathrm{in}}y_{ml,\mathrm{in}}z_{\max} = \sum_{2}^{nk-1}\sum_{2}^{j_{ml,i}}(\bar{u}_eA_{e,x} + \bar{v}_eA_{e,y}) \qquad (11)$$

where $nk-2$ is the number of cells in the spanwise (z) direction. $j_{ml}-1$ is the number of cells in the URANS region near the lower wall and $A_{e,x}$ and $A_{e,y}$ are the x and y component of the east (i.e. $i+1/2$) surface area of a control volume ($A_e = [A^2_{e,x} + A^2_{e,y}]^{1/2}$). Unless otherwise stated, the location of the matching plane is computed as described above.

For a configuration, where the spanwise direction is not a homogeneous one, this can be done locally for each k (k denotes the control volume index in the spanwise direction), i.e.

$$U_{b,\mathrm{in},k}y_{ml,\mathrm{in},k}\Delta z = \sum_{2}^{j_{ml,i,k}}(\bar{u}_eA_{e,x} + \bar{v}_eA_{e,y}) \qquad (12)$$

The location of the matching plane near the lower and upper wall at one instant computed from equation 11 is shown in figure 15 (actually $j_{ml,i}$ is computed by taking the averaging of the three last time steps).

The predicted pressure coefficients in figure 16a are well in agreement with experiments in the first part of the expansion. Further downstream the predicted C_p is too large. Also the pressure coefficient predicted in Kaltenbach *et al.* (1999) is in this region slightly higher than the experimental values (but smaller than the present predictions). It is suggested in Kaltenbach *et al.* (1999) that part of the discrepancy can be attributed to three-dimensional effects in the middle part of the expansion, giving bulk velocities in the center plane which are some 5% too high.

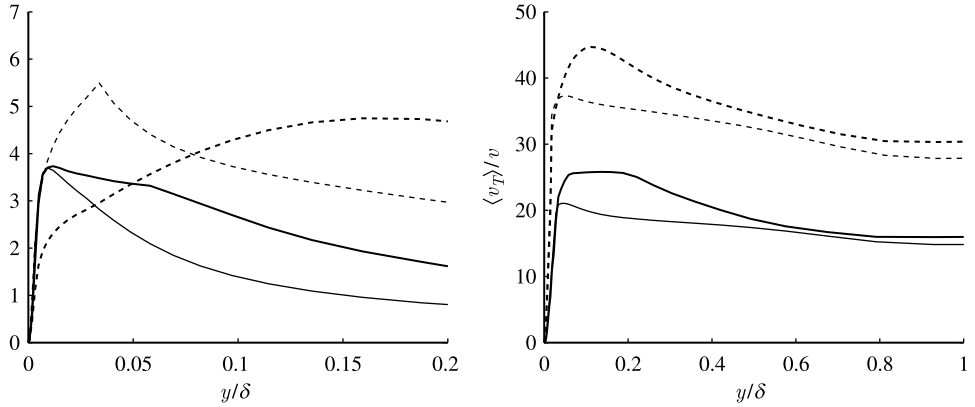

(a) $Re_\tau = 2000$. Turbulent kinetic energy scaled with $u^2_{*,w}$. Solid lines: modelled; dashed lines: resolved.

(b) Turbulent viscosity. Solid lines: $Re_\tau = 2000$; dashed lines: $Re_\tau = 4000$.

Figure 10. Channel flow. Streamwise periodic boundary conditions. $y^+_{ml} \simeq 60$. Thin lines: with forcing conditions; thick lines: without forcing conditions.

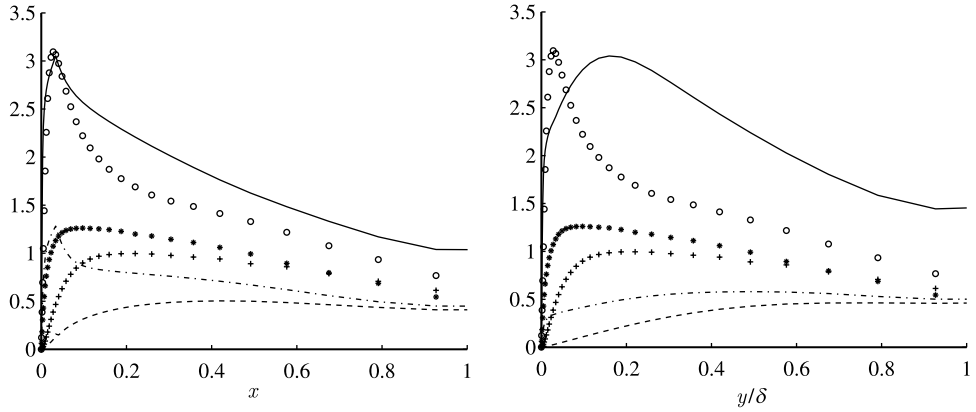

(a) With forcing conditions. (b) Without forcing conditions.

Figure 11. Channel flow. Resolved RMS fluctuations scaled with $u_{*,w}$ at $Re_\tau = 2000$. Solid lines: streamwise; dashed lines: wall-normal; dash-dotted: spanwise. $y_{ml} = 62$. Markers: present DNS.

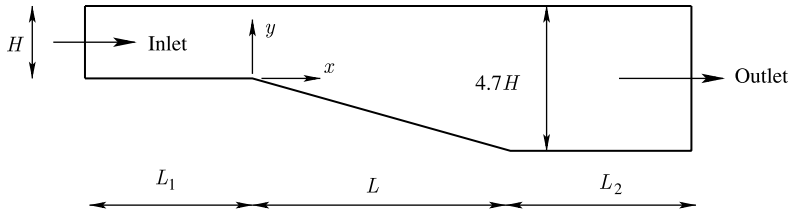

Figure 12. Plane asymmetric diffuser (not to scale). $L_1 = 7.9H$, $L = 21H$, $L_2 = 28H$. The spanwise width is $z_{\max} = 4H$. The origin of $x - y - z$ is at the lower wall at the entrance of the diffuser.

Figure 16b shows that the predicted recirculation region along the lower wall is too strong compared with experiments. The predicted skin friction goes negative at $x/H = 1.5$ and assumes positive value at $x/H \simeq 32.5$. For $x/H > 20$, the predicted skin friction along the lower wall agrees well with experiments. At the upper wall the predicted skin friction agrees well except at the start of the expansion.

The predicted shear stresses, both resolved and modelled, are compared with experiments in figure 17. In the beginning of the expansion the predicted stresses near the lower wall are much large. The magnitude of the modelled shear stresses at $x/H = 3$ and $x/H = 6$ is similar to that in the experiments, but the resolved stresses are approximately twice as large as the experimental values. It may seem somewhat surprising that the predicted shear stresses are that different from the experimental ones, and still the agreement between the predicted and velocities is that good. The reason is that in regions, where the resolved stress is large, it is not a dominating term. For example at $x/H = 3$, at the y location of maximum shear stress the advective term $\langle\bar{u}\rangle\partial\langle\bar{u}\rangle/\partial x$ is three times larger than the y-gradient of the resolved shear stress and the magnitude of the pressure gradient $\partial\bar{p}/\partial x$ is similar to that of

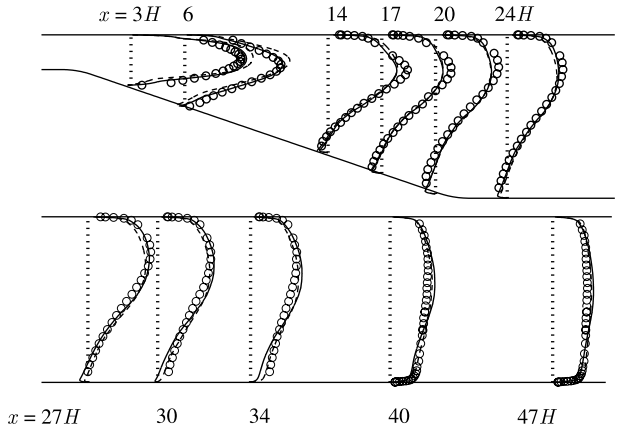

Figure 13. Diffuser. $\langle\bar{u}\rangle/U_{b,\text{in}}$ profiles. Solid lines: with forcing conditions; dashed lines: without forcing conditions; markers: experiments (Buice and Eaton 1997).

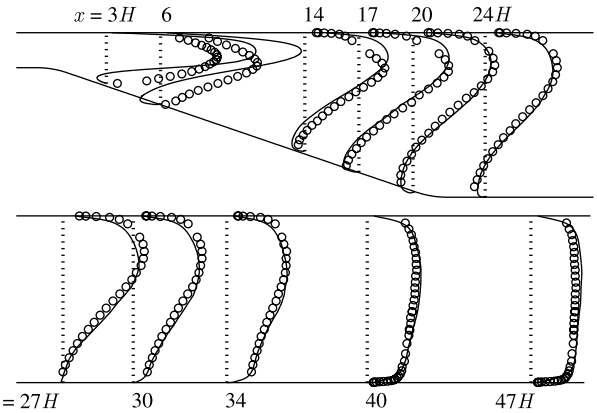

Figure 14. Diffuser. $\langle\bar{u}\rangle/U_{b,\text{in}}$ profiles. LES with a one-equation k_{sgs} model. Solid lines: LES; markers: experiments (Buice and Eaton 1997).

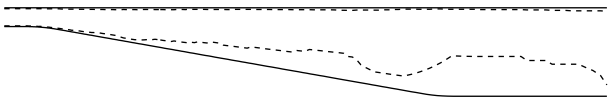

Figure 15. Location of matching planes at one instant.

$-\partial\langle u'v'\rangle/\partial y$. From $x/H = 13$ and downstream the agreement between predicted and experimental shear stresses is much better. It is interesting to note that in the separation region along the lower wall, the modelled stress dominate whereas, outside the separation region the resolved stress is much larger than the modelled one.

Figure 18 shows the turbulent viscosities. The magnitudes of ν_T/ν are quite large. For example, the peak value at $x/H = 20$ is $\nu_{T,\max}/\nu \simeq 380$, which is similar to what has been found in RANS computations (Apsley and Leschziner 1999). This can be compared with the peak value in the straight channel at $x = -7H$ (upstream of the diffuser part) where $\nu_{T,\max}/\nu \simeq 12$. The high values of ν_T was expected, of course, considering that the larger part of the turbulence in this region is modelled rather than resolved. In the well-resolved LES of the asymmetric diffuser presented in Kaltenbach *et al.* (1999) the ratio ν_{sgs}/ν did not exceed 5 in the recirculation region.

All results presented so far have been obtained by defining the location according to equation 11. One side effect of this definition is that the larger part of the separation region is treated in URANS mode. In the Introduction, it was explained that large turbulent scales are usually conveniently captured by LES. The separation is indeed dominated by large scales which we would like to cover with the LES region. Figure 19 presents predictions in which the matching plane has been set to a constant grid line at both upper and lower wall. At the inlet $y^+ = 34$ (corresponds to $y/H = 0.032$) which gives 10 ten cells in the wall-normal direction in each URANS region. The relative height of each URANS region is constant for every x, i.e. $|y_{ml} - y_{\text{wall}}|/h(x)$ is approximately constant ($h(x)$ denotes the local height of the diffuser). In this way the separation region is covered by the LES region. As can be seen from figure 19 the results are poor. When forcing is used at the matching plane, slightly better results are obtained, but the agreement with experiments is still poor.

6. Concluding remarks

Hybrid LES-RANS has been used for simulating the flow in a plane channel and an asymmetric diffuser. One problem in standard hybrid LES-RANS is that the turbulent structural information supplied by the URANS region to the LES region across the matching plane is very poor. To solve this problem a new approach in which turbulent fluctuations are added at the interface (forcing conditions) was investigated in the present study.

It was found that the fully developed flow in channels is well predicted by hybrid LES-RANS when forcing conditions were used. Without forcing conditions, the results were not that good, but still much better than LES.

The diffuser flow was fairly well predicted both with and without forcing conditions. In Apsley and Leschziner (1999) this flow was investigated evaluating different RANS models (linear and non-linear eddy-viscosity models as well as Reynolds stress transport models). The agreement between the present hybrid LES-RANS (with location of matching plane defined from equation 11) and experiments is better than for most RANS models investigated in Apsley and Leschziner (1999). Furthermore, the recovery of the boundary layer is also much better predicted with hybrid LES-RANS compared to the RANS predictions Apsley and Leschziner (1999). It is very difficult to accurately predict the recovery rate with RANS. It should of course be kept in mind that three-dimensional, time-dependent hybrid LES-RANS simulations require orders of magnitudes more CPU time than 2D RANS.

In the present study, the added turbulent fluctuations were taken from a DNS simulation of a generic boundary

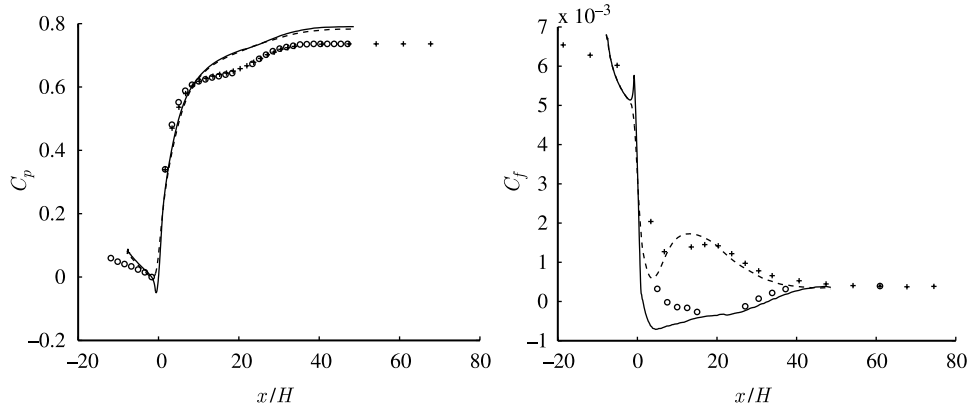

(a) Pressure coefficient. (b) Friction coefficient.

Figure 16. Diffuser. Pressure and skin coefficients. Forcing conditions. Solid line: lower wall; dashed lines: upper wall; markers: experiments (Buice and Eaton 1997).

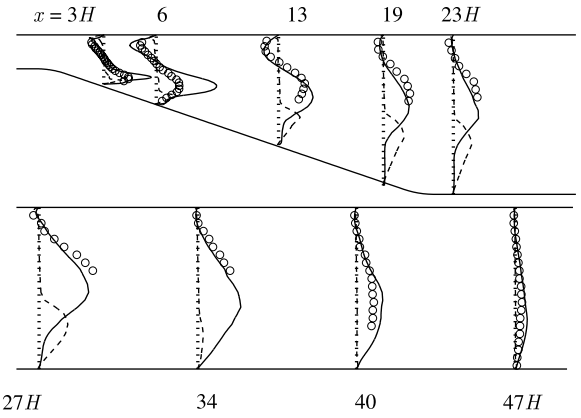

Figure 17. Diffuser. Profiles of turbulent shear stresses. Forcing conditions. Solid lines: resolved $\langle -u'v'\rangle/U_{b,\mathrm{in}}^2$; dashed lines: modelled $2\langle\nu_t\bar{s}_{12}\rangle/U_{b,\mathrm{in}}^2$. The lower profiles have been multiplied by two.

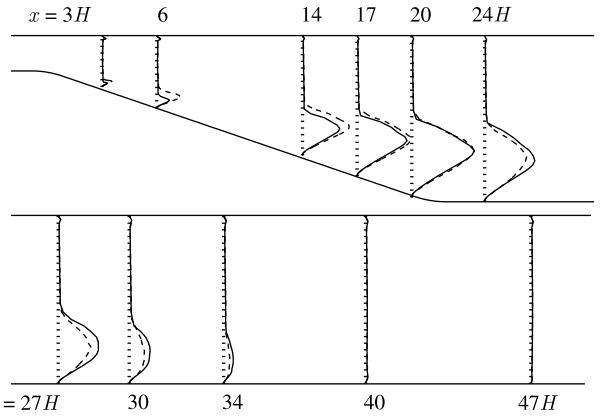

Figure 18. Diffuser. Turbulent viscosity $\langle\nu_T\rangle/\nu$. Solid lines: with forcing; dashed lines: without forcing.

layer. As an alternative, turbulent instantaneous fluctuations can be generated assuming isotropic turbulence with a modified von Kármán spectrum. This approach is investigated in Davidson and Billson (2004).

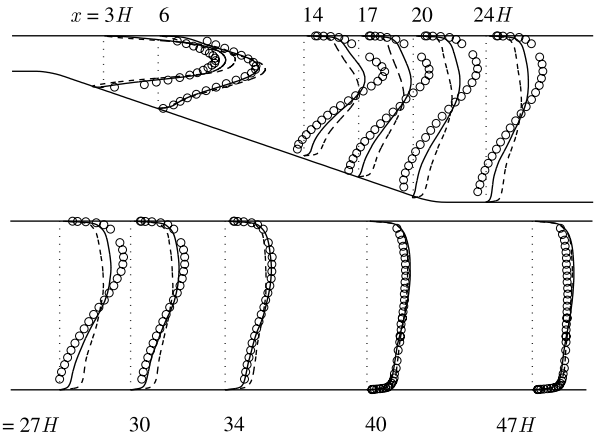

Figure 19. Diffuser. $\langle\bar{u}\rangle/U_{b,\mathrm{in}}$ profiles. Matching plane fixed at one grid line. Solid lines: with forcing conditions; dashed lines: without forcing conditions; markers: experiments (Buice and Eaton 1997).

Acknowledgements

This work was financed by the FLOMANIA project (Flow Physics Modelling—An Integrated Approach) and is a collaboration between Alenia, AEA, Bombardier, Dassault, EADS-CASA, EADS-Military Aircraft, EDF, NUMECA, DLR, FOI, IMFT, ONERA, Chalmers University, Imperial College, TU Berlin, UMIST and St Petersburg State University. The project is funded by the European Union and administrated by the CEC, Research Directorate-General, Growth Programme, under Contract No. G4RD-CT2001-00613.

References

Alfredsson, H. and Johansson, A.V., On the detection of turblence-generating events. *J. Fluid Mech.*, 1984, **139**, 325–346.

Apsley, D.D. and Leschziner, M.A., Advanced turblence modelling of separated fbw in a diffuser. *Flow Turbul. Combust.*, 1999, **63**, 81–112.

Baggett, J.S., Some modeling requirements for wall models in large eddy simulation. *Annual Research Briefs*, pp. 123–134, 1997 (Center for Turbulent Research, Stanford University/NASA Ames Research Center).

Batten, P., Goldberg, U. and Chakravarthy, S., Interfacing statistical turbulence closures with large-eddy simulation. *AIAA J.*, 2004, **42**(3), 485–492.

Buice, C.U. and Eaton, J.K., Experimental investigation of flow through an asymmetric plane diffuser. Report No. TSD-107, Thermosciences Division, Department of Mechanical Engineering, Stanford University, Stanford, California 94305, 1997.

Dahlström, S., Large Eddy simulation of the flow around a high-lift airfoil, Ph. D thesis, Department of Thermo and Fluid Dynamics, Chalmers University of Technology, Göteborg, Sweden, 2003.

Dahlström, S. and Davidson, L., Hybrid RANS-LES with additional conditions at the matching region. In *Turbulence Heat and Mass Transfer 4*, edited by K. Hanjalić, Y. Nagano and M.J. Tummers, pp. 689–696, 2003 (Begell House, inc: New York, Wallingford (UK)), www.tfd.chalmers.se/~lada.

Davidson, L. and Peng, S.-H., Hybrid LES-RANS: A one-equation SGS model combined with a $k-\omega$ model for predicting recirculating flows. *Int. J. Numer. Methods Fluids*, 2003, **43**, 1003–1018.

Davidson, L., Cokljat, D., Fröhlich, J., Leschziner, M.A., Mellen, C. and Rodi, W. (Eds.) *LES-FOIL: Large Eddy Simulation of Flow Around a High Lift Airfoil*, Notes on Numerical Fluid Mechanics, Vol. 83, Springer Verlag, 2003.

Davidson, L., Hybrid LES-RANS: A combination of a one-equation SGS model and a $k-\omega$ model for predicting recirculating flows. in *ECCOMAS CFD Conference*, 2001 Swansea, UK, www.tfd.chalmers.se/~lada.

Davidson, L. and Billson, M., Hybrid LES/RANS using synthesized turbulence for forcing at the interface. In *ECCOMAS 2004*, edited by P. Neittaanmäki, T. Rossi, S. Korotov, E. O¯nate, J. Périaux and D. Knörzer, July 24–28, Finland, 2004, www.tfd.chalmers.se/~lada.

Emvin, P., The full multigrid method applied to turbulent flow in ventilated enclosures using structured and unstructured grids, PhD thesis, Department of Thermo and Fluid Dynamics, Chalmers University of Technology, Göteborg, 1997.

Hamba, F., An approach to hybrid RANS/LES calculation of channel flow. In *Engineering Turbulence Modelling and Experiments*, edited by W. Rodi and N. Fueyo, pp. 297–305, 2003 (Elsevier).

Kaltenbach, H.J., Fatica, M., Mittal, R., Lund, T.S. and Moin, P., Study of fbw in plane asymmetric diffuser using large-eddy simulation. *J. Fluid Mech.*, 1999, **390**, 151–186.

Kim, J., Moin, P. and Moser, R., Turbulence statistics in fully developed channel fbw at low Reynolds number. *J. Fluid Mech.*, 1987, **177**, 133–166.

Krajnović, S. and Davidson, L., Large eddy simulation of the flow around a bluff body. *AIAA J.*, 2002, **40**(5), 927–936.

Krajnović, S. and Davidson, L., Numerical study of the flow around the bus-shaped body. *ASME J. Fluids Eng.*, 2003, **125**, 500–509.

Krajnović, S. and Davidson, L., Large eddy simulation of the flow around an Ahmed body, in *2004 ASME Heat Transfer/Fluids Engineering Summer Conference*, Charlotte, USA, 2004, www.tfd.chalmers.se/~lada.

Mellen, C.P., Fröhlich, J. and Rodi, W., Lessons from LESFOIL project on large eddy simulation of flow around an airfoil. *AIAA J.*, 2003, **41**(4), 573–581.

Moser, R.D., Kim, J.D. and Mansour, N., Direct numerical simulation of turbulent channel fbw up to $Re_\tau = 590$. *Phys. Fluids A*, 1999, **11**, 943–945.

Nikiton, N.V., Nicoud, F., Wasistho, B., Squires, K.D. and Spalart, P., An approach to wall modeling in large-eddy simulations. *Phys. Fluids A*, 2000, **12**(7), 1629–1632.

Piomelli, U., Balaras, E., Pasinato, H., Squire, K.D. and Spalart, R., The inner-outer layer interface in large-eddy simulations with wall-layer models. *Int. J. Heat Fluid Flow*, 2003, **24**, 538–550.

Robinson, S.R., Coherent motions in the turbulent boundary layer. *Annu. Rev. Fluid Mech.*, 1991, **23**, 601–639.

Rodi, W., Ferziger, J.H., Breuer, M. and Pourquié, M., Status of large-eddy simulations: Results of a workshop. *Fluids Eng.*, 1997, 248–262.

Spalart, P.R., Jou, W.-H., Strelets, M. and Allmaras, S.R., Comments on the feasability of LES for wings and on a hybrid RANS/LES approach. In *Advances in LES/DNS, First International Conference on DNS/LES*, edited by C. Liu and Z. Liu, 1997 (Louisiana Tech University, Greyden Press).

Spalart, P.R., Strategies for turbulence modelling and simulations. *Int. J. Heat Fluid Flow*, 2000, **21**, 252–263.

Strelets, M., Detached eddy simulation of massively separated flows, AIAA paper 2001–0879, Reno, NV, 2001.

Temmerman, L. and Leschziner, M.A., *A-priori* studies of near-wall RANS model within a hybrid LES/RANS scheme. In *Engineering Turbulence Modelling and Experiments, 5*, edited by W. Rodi and N. Fueyo, pp. 317–326, 2002 (Elsevier).

Tucker, P., Differential equation based length scales to improve DES and RANS simulations, AIAA paper 2003-3968, 16th AIAA CFD Conference, 2003.

Tucker, P. and Davidson, L., Zonal k-1 based large eddy simulation. *Comput. Fluids*, 2004, **33**(2), 267–287.

Xiao, X., Edwards, J.R. and Hassan, H.A., Inflow boundary conditions for LES/RANS simulations with applications to shock wave boundary layer interactions, AIAA paper 2003–0079, Reno, NV, 2003.